Chapter 2

Uplift and subsidence associated with the great Aceh–Andaman earthquake of 2004

Aron J. Meltzner, Kerry Sieh, Michael Abrams, Duncan C. Agnew,

Kenneth W. Hudnut, Jean-Philippe Avouac, and Danny H. Natawidjaja

Reprinted from the *Journal of Geophysical Research*

Volume 111, B02407, doi:10.1029/2005JB003891

February 2006

with modifications to the Supplementary Files

Uplift and subsidence associated with the great Aceh-Andaman earthquake of 2004

Aron J. Meltzner,[1] Kerry Sieh,[1] Michael Abrams,[2] Duncan C. Agnew,[3]
Kenneth W. Hudnut,[4] Jean-Philippe Avouac,[1] and Danny H. Natawidjaja[5]

Received 20 June 2005; revised 5 October 2005; accepted 22 November 2005; published 15 February 2006.

[1] Rupture of the Sunda megathrust on 26 December 2004 produced broad regions of uplift and subsidence. We define the pivot line separating these regions as a first step in defining the lateral extent and the downdip limit of rupture during that great $M_w \approx 9.2$ earthquake. In the region of the Andaman and Nicobar islands we rely exclusively on the interpretation of satellite imagery and a tidal model. At the southern limit of the great rupture we rely principally on field measurements of emerged coral microatolls. Uplift extends from the middle of Simeulue Island, Sumatra, at ~2.5°N, to Preparis Island, Myanmar (Burma), at ~14.9°N. Thus the rupture is ~1600 km long. The distance from the pivot line to the trench varies appreciably. The northern and western Andaman Islands rose, whereas the southern and eastern portion of the islands subsided. The Nicobar Islands and the west coast of Aceh province, Sumatra, subsided. Tilt at the southern end of the rupture is steep; the distance from 1.5 m of uplift to the pivot line is just 60 km. Our method of using satellite imagery to recognize changes in elevation relative to sea surface height and of using a tidal model to place quantitative bounds on coseismic uplift or subsidence is a novel approach that can be adapted to other forms of remote sensing and can be applied to other subduction zones in tropical regions.

Citation: Meltzner, A. J., K. Sieh, M. Abrams, D. C. Agnew, K. W. Hudnut, J.-P. Avouac, and D. H. Natawidjaja (2006), Uplift and subsidence associated with the great Aceh-Andaman earthquake of 2004, *J. Geophys. Res.*, *111*, B02407, doi:10.1029/2005JB003891.

1. Introduction

[2] The 26 December 2004 $M_w \approx 9.2$ Aceh-Andaman earthquake resulted from slip on the subduction interface between the Indo-Australian plate and the Burma microplate below the Andaman and Nicobar islands and Aceh province, Sumatra (Figure 1). The distribution of aftershocks (e.g., from U.S. Geological Survey, available at http://neic.usgs.gov/neis/poster/2004/20041226.html) suggests that the rupture extended over a distance of 1500 km (measured parallel to the arc), but seismic inversions for this event are nonunique and cannot resolve many details of slip, especially along the northern portion of the rupture [e.g., *Ammon et al.*, 2005]. Furthermore, considering that slip north of ~9°N appears to have generated little or no seismic radiation [*Lay et al.*, 2005; *Ammon et al.*, 2005], seismic inversions will only provide a minimum constraint on the extent and amount of slip, and geodetic inversions will be required to provide a maximum (and perhaps more accurate) constraint. However, inversions of the sparse geodetic data that were available prior to this study provided only limited constraints on the amount and distribution of slip [e.g., *Subarya et al.*, 2006].

[3] In this paper, we combine satellite imagery and ground observations to map the extent of coseismic uplift and for some locations to constrain or estimate the magnitude of uplift or subsidence. In general, for a subduction megathrust earthquake, coseismic deformation of the upper plate can be modeled using an elastic slip dislocation model [e.g., *Plafker and Savage*, 1970; *Plafker*, 1972; *Natawidjaja et al.*, 2004]; one simple model is shown in Figure 2. To a first order approximation, during the interseismic period the portion of the upper plate overlying the locked subduction interface is gradually depressed, while the region landward of the locked fault zone bows upward slightly; then, during the earthquake the region above the updip portion of the rupture recovers the elastic strain stored during the interseismic period and experiences sudden coseismic uplift, whereas the downdip end of the rupture and adjacent regions subside. A small fraction of the coseismic uplift may reflect permanent strain accumulation in the forearc region. Although no modeling is presented in this paper, the region of coseismic uplift approximates the north-to-south rupture extent and demarcates a minimum downdip width of faulting. Resolution of the pattern of uplift, using a dense

[1]Tectonics Observatory, Division of Geological and Planetary Sciences, California Institute of Technology, Pasadena, California, USA.
[2]Jet Propulsion Laboratory, California Institute of Technology, Pasadena, California, USA.
[3]Scripps Institution of Oceanography, University of California, San Diego, La Jolla, California, USA.
[4]U.S. Geological Survey, Pasadena, California, USA.
[5]Research Center for Geotechnology, Indonesian Institute of Sciences, Bandung, Indonesia.

0148-0227/06/2005JB003891$09.00

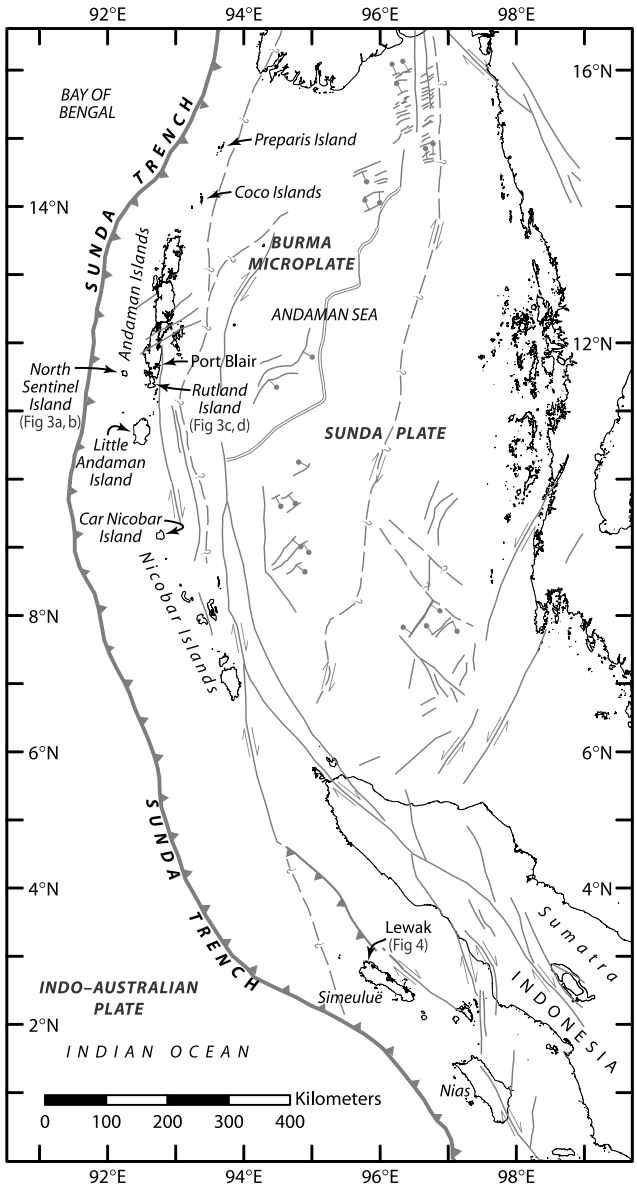

Figure 1. Overview map showing faults and plate boundaries from *Curray* [2005], places named in the text, and the general locations of Figures 3 and 4.

array of geodetic data points, can provide robust constraints on the coseismic slip distribution.

2. Procedure

2.1. Coral Background

[4] Our work combines two types of observations to arrive at a comprehensive map of uplift and subsidence associated with the 2004 earthquake and, in particular, of the "pivot line" separating the regions of uplift and subsidence. Fundamental to these techniques is the presence of coral heads and reefs surrounding many of the Andaman and Nicobar islands and much of the Indonesian archipelago. Each coral head or microatoll grows up to a certain elevation with respect to the annual lowest tides at a given locality. Above this maximum elevation, called the highest level of survival (HLS), a coral cannot survive and grow [*Taylor et al.*, 1987]. Corals living beneath the HLS grow both outward and upward (typically at rates on the order of 1 cm/yr) until the tops of the coral heads reach the HLS; subsequently, their tops die, and they are limited to horizontal growth. Although the elevation of the HLS of a coral relative to sea level is not strictly defined and varies according to genus or species, it nevertheless appears that HLS "tracks" lowest low-water levels with a sensitivity of a few centimeters [*Zachariasen et al.*, 2000]. A coral that is stable relative to the annual lowest tides should have a remarkably flat top. Thus coral microatolls can record tectonic uplift or subsidence. In addition, satellite imagery of coral reefs is useful for assessing differences in relative sea level, as the color and brightness of a reef in an image is strongly dependent upon the depth of water above the reef.

2.2. Analysis of Satellite Imagery

[5] Because many species of coral grow upward to near the annual low-tide level, they are sensitive to relative sea level changes of several centimeters or more. The water penetration depths for satellite images are typically tens of centimeters to a few meters [*Miller et al.*, 2005]. In standard analyses of false color satellite images, coral reefs appear to grade from a deep bluish color when submerged in comparatively deep water to a lighter, brighter blue when submerged under very shallow water to a pinkish or reddish white when exposed subaerially. (In these false color images, vegetation appears red; algae, which also appears red in false color, will not grow on living coral but will grow in the intertidal zone on coral heads that have been exposed and died; we interpret the reddish color on the coral reefs to result from algae growing on uplifted and exposed coral.)

[6] We examined Advanced Spaceborne Thermal Emission and Reflection Radiometer (ASTER), SPOT, IKONOS, QuickBird, and Landsat images of the region around the December 2004 rupture, identifying areas with different amounts of reef or land exposure in the different images. We compared satellite images acquired prior to the earth-

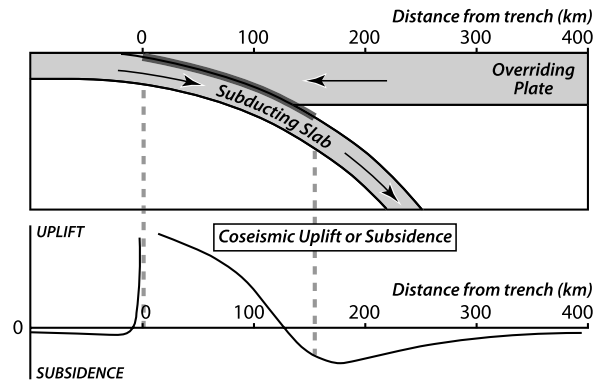

Figure 2. Generic elastic slip dislocation model. (top) Cross-section view across the subduction zone with the shaded parts corresponding to the lithosphere. The thick line represents the locked interface, which slips during the giant megathrust earthquakes. (bottom) Hypothetical pattern of coseismic uplift and subsidence and its geometrical relationship to slip on the locked interface. In a real case, factors including fault dip angle and slip distribution affect the actual pattern of uplift and subsidence.

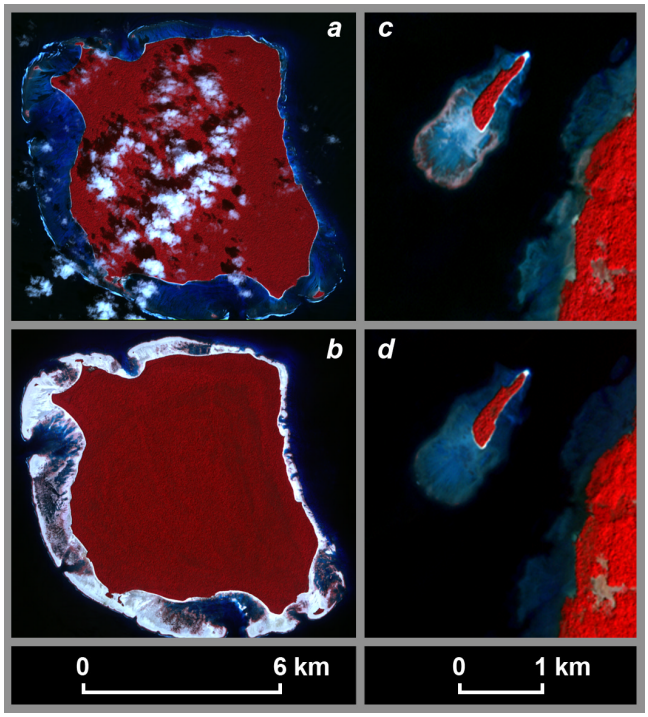

Figure 3. (a) Preearthquake and (b) postearthquake Advanced Spaceborne Thermal Emission and Reflection Radiometer (ASTER) images of North Sentinel Island, showing emergence of the coral reef surrounding the island. The tide was 30 ± 14 cm lower in the preearthquake image (acquired 21 November 2000) than in the postearthquake image (acquired 20 February 2005), requiring a minimum of 30 cm of uplift at this locality. Observations from an Indian Coast Guard helicopter on the northwest coast of the island suggest that the actual uplift is on the order of 1–2 m at this site [*Bilham et al.*, 2005]. (c) Preearthquake and (d) postearthquake ASTER images of a small island off the northwest coast of Rutland Island, 38 km east of North Sentinel Island, showing submergence of the coral reef surrounding the island. The tide was higher in the preearthquake image (acquired 1 January 2004) than in the postearthquake image (acquired 4 February 2005), requiring subsidence at this locality. The pivot line must run between North Sentinel and Rutland islands. Note that the scale for the North Sentinel Island images differs from that for the Rutland Island images.

quake with images acquired between 28 December 2004 and 26 March 2005 (we looked at images acquired as late as 15 August 2005 for Car Nicobar). After stretching and normalizing the color distribution in each image we relied on changes in the color and brightness of the reefs among the images to assess the relative levels of reef exposure. Fortunately, in most cases these differences in color and brightness were pronounced enough to be fairly insensitive to small variations in the overall color representations of the images. We then used a tidal model (discussed in Appendix A) to determine the relative sea surface height (SSH) at each location at the acquisition time of each image. The 2σ uncertainty of the tidal model is roughly ±10 cm, so the calculated difference between two SSHs for a given location should be accurate to ~14 cm or better. However, a ±14 cm (2σ) uncertainty associated with the overall satellite imagery method would be conservative; because we have only used image comparisons in which the difference in color or brightness is unambiguous, this effectively places a "buffer" of at least a few centimeters on our stated maximum or minimum bounds. Hence an appropriate 2σ uncertainty for a stated bound should be significantly less than 14 cm. Nonetheless, because we cannot quantify the aforementioned "buffer," we will retain the conservative 14 cm (2σ) uncertainty for use in this paper.

[7] The sensitivities of the satellite imagery method and of the tidal model were verified by comparing the apparent relative exposures among preearthquake images in numerous locations where multiple images were acquired prior to the earthquake. In looking only at images acquired between 2000 and 2004, we could neglect both interseismic vertical deformation and potential growth of the corals, which should be well within the uncertainty of the tidal model. Presumably, any differences in reef color or brightness among these images should be due solely to differences in the tides. In support of both the method and the tidal model, SSH differences as small as 5–10 cm (less than the stated 2σ uncertainty) were commonly recognizable among the images of a particular location, with lower SSHs corresponding to more brightly colored reefs.

[8] In order to document uplift of a reef we looked for a postearthquake image with more reef exposure than a preearthquake image of the same area taken at a lower tide; in that case, the difference in SSH between the two images can be taken as a minimum constraint on the amount of uplift. Similarly, to document subsidence, we looked for a preearthquake image with more reef exposure than a postearthquake image at a lower tide; in this case, the difference in SSH is a minimum constraint on the amount of subsidence. An example of each exercise is presented in Figure 3. In addition, we were also able to demonstrate subsidence in well-drained coastal areas that were not regularly flooded prior to December 2004 but which have been submerged since the earthquake.

2.3. In Situ Analysis of Coral Microatolls

[9] In addition to the satellite-based observations a set of field measurements of uplift was made on emerged coral heads around Simeulue Island, off the coast of Sumatra, by K. Sieh, D. H. Natawidjaja, J. Galetzka, and others (e.g., see Figure 4). Prior to the 26 December 2004 earthquake each of these corals was living, and the tops of each coral head coincided with the preearthquake HLS. During the earthquake these corals were uplifted, and the portions of each coral head now exposed to air would have been killed. Over the following days and weeks each time a new low tide was reached, an additional lower portion of the microatoll was exposed and died. For each microatoll a measurement was made of the vertical distance between the (now dead) top of the coral head and the present HLS, which was readily identifiable in the field by the pattern of algae growth; algae will not grow on living corals, but it was observed in many places to grow immediately above the coral HLS, extending as much as a half meter above the coral HLS. If the annual lowest tide (in the year preceding the earthquake) was equal to the lowest low tide that happened to occur in the time between the earthquake and

Figure 4. A *Porites* coral microatoll that died because of emergence on 26 December 2004 at Lewak, on Simeulue. The flat top of the coral head marks the preearthquake highest level of survival (HLS), and the new HLS is near the base of the coral (there is still living tissue on the coral, just at the water line). The pronounced horizontal line 10–15 cm below the top of the coral is the uppermost limit of algae growth; this level is not used for our measurement. The difference in elevation between the preearthquake HLS and the new HLS is 44 cm. Actual uplift at this site, which includes the 44 cm measured in the field plus a tidal correction of 2 cm (discussed in the text), is 46 cm. Photo courtesy of J. Galetzka, taken at very low tide.

the field measurement (most of the measurements were made on 17 or 18 January 2005), then the vertical distance between the preearthquake HLS and the HLS at the time of the measurement would equal the amount of uplift at the location. However, because the lowest tide between 26 December 2004 and the time of measurement was slightly higher than the annual lowest tide, a small correction needed to be made. For each location the tidal model (discussed in Appendix A) was used to calculate the difference between (1) the lowest low tide in the year preceding the earthquake and (2) the lowest low tide in the period between the earthquake and the time of the measurement; this difference was added to the in situ measurement of uplift. In general, this difference was less than 5 cm.

3. Results and Discussion

[10] We were able to apply the satellite imagery technique throughout the rupture area where there was available coverage both before and after the earthquake and where there were markers that were clearly exposed to different extents in the various images (any before-and-after image pair for which the relative extents of reef exposure could not be determined without ambiguity was discarded). We have near-complete coverage of the Andaman Islands, partial coverage of the Nicobar Islands, and spotty coverage in Sumatra. Because the climate in January to March is relatively dry in the Andamans but is wetter closer to the equator, it was increasingly difficult toward the south to acquire cloud-free images between 26 December 2004 and 28 March 2005. We supplemented the satellite-based work with the in situ measurements of uplift on the coral heads in northwestern Simeulue, where it was especially difficult to acquire clear postearthquake images prior to the subsequent 28 March 2005 Simeulue-Nias earthquake.

[11] Our results are summarized in Figure 5 and auxiliary material[1] Tables S1–S3. Broadly, the northern and western Andaman Islands were uplifted, whereas the southern and eastern portion of the islands subsided. The pivot line separating uplift from subsidence is nearest the Sunda Trench at about 11.4°N, but it trends obliquely away from the trench to the north and south. Farther south, all of the Nicobar Islands and northwestern mainland Sumatra subsided, so the location of the pivot line between 10°N and just north of 3°N is bounded only to the east. As seen from the field measurements of coral microatolls, there is a sharp uplift gradient across Simeulue, with the western tip of the island up 1.5 m and the southeastern 30 km of the 100 km long island having subsided. The pivot line is most tightly constrained in the Andaman Islands and on Simeulue.

[1] Auxiliary material is available at ftp://ftp.agu.org/apend/jb/2005JB003891.

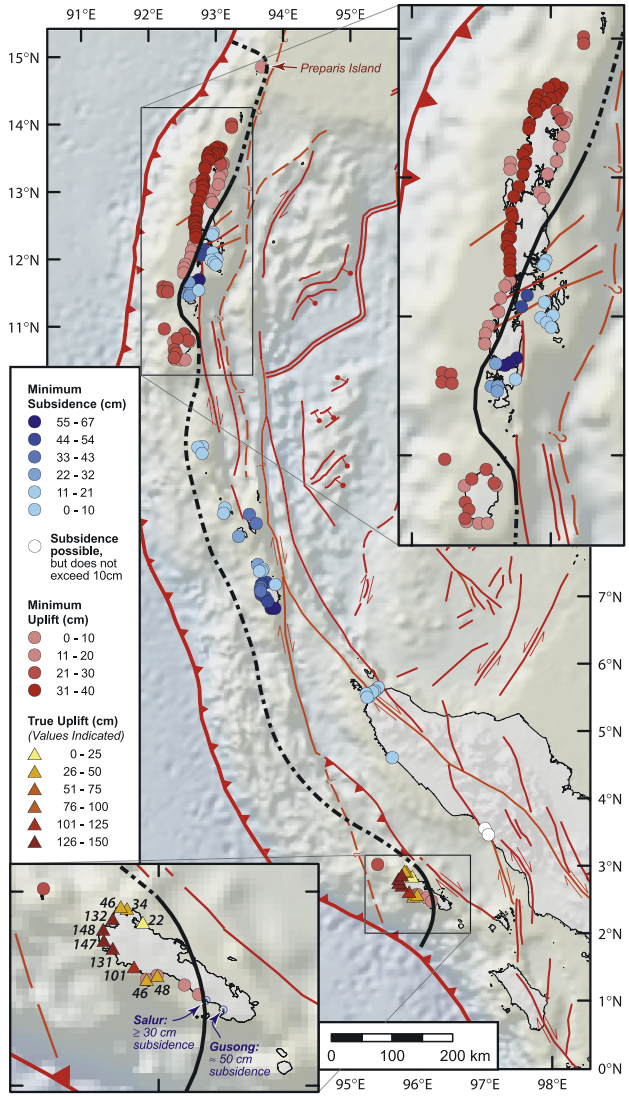

Figure 5. Summary map showing minimum constraints on uplift or subsidence from satellite imagery, as well as field measurements of uplift and subsidence on Simeulue. Also shown are faults from *Curray* [2005] and our best estimate of the location of the pivot line. The pivot line is shown as a solid thick black line where its location is more tightly constrained and as a dashed line where it is more poorly constrained. Estimate of subsidence at Busung, Gusong Bay, Simeulue, is from R. Peters (http://walrus.wr.usgs.gov/news/reportsleg1.html). The four imagery-based uplift constraints on Simeulue (pink circles) span both the 2002 and 2004 earthquakes and thus represent minimum net uplift for the two events. See text and Table S1 for more details.

[12] Resolution of slip at the northernmost end of the rupture is based upon a single datum at Preparis Island (Figure 5). Unfortunately, the only preearthquake ASTER image of Preparis Island is marred by high atmospheric water content, which affects the color of the image. While we do not feel this warrants discarding the datum, and while analysis of a (lower resolution) Landsat image of the region acquired on 11 January 2002 also supports minor (20–30 cm) uplift, we concede that this datum is not as robust as the majority of our imagery-based observations. Attempts to perform a comparable analysis using Envisat synthetic aperture radar (SAR) images were inconclusive (E. Fielding, personal communication, 2005; M. Tobita, personal communication, 2005).

[13] Concerns about the northernmost data point aside, our observations suggest that the 26 December 2004 rupture extended from under Simeulue Island northward to Preparis Island of Myanmar (Burma), near latitude 15°N. Although different authors have measured the length of the rupture differently, measured parallel to the arc (as opposed to along a straight line connecting the rupture endpoints), the rupture is ~1500 km long if it extends from northern Simeulue to latitude 14°N, and it is ~1600 km long if it extends to 15°N. Our preferred northern limit (15°N) is at least 100 km north of the northern extent of rupture suggested by aftershock locations (e.g., from the U.S. Geological Survey) and by inversions of seismic data [e.g., *Ammon et al.*, 2005]. However, in addition to the uplift directly over the rupture patch, minor uplift would be expected on the updip edge as well as beyond the northern and southern edges of the rupture (V. Gahalaut, personal communication, 2005). If real, the small amount of uplift at Preparis Island does not require that slip along the underlying fault plane propagated that far north, only nearly so.

[14] We must also consider the possibility of interseismic and postseismic slip being included in our observations. While the amount of interseismic slip that may have occurred within the period of our observations (less than 5 years) is probably a negligible fraction of the coseismic slip, postseismic slip may be significant. For example, continuous GPS data from the SAMP (Sampali) site near Medan along the northeast coast of Sumatra reveal a clear record of coseismic slip and postseismic relaxation: The daily time series from SAMP shows a coseismic horizontal displacement of 13.8 cm which increased logarithmically by about 15% over 15 days and by about 25% over 60 days following the earthquake [*Subarya et al.*, 2006]. Similarly, *Vigny et al.* [2005] report that Phuket, Thailand, moved 1.25 times the initial coseismic displacement there during the first 50 days after the earthquake, and *Gahalaut et al.* [2006] observed that during the period 11–22 January 2005, Port Blair moved horizontally by 3.5 cm in the same direction as that of the coseismic displacement. Hence our result at each location may be dependent upon the date of the postearthquake observation. Instead of attempting to model the separate contributions of coseismic and postseismic slip to each of our observations, we simply present the dates of each observation along with the respective datum (Tables S1–S3), and we leave it to the discretion of any users of our data to model the data as they see fit.

[15] In addition to postseismic slip following the 2004 earthquake, coseismic slip from an additional earthquake may have been captured by our imagery observations on Simeulue island. While we did not examine images of Simeulue captured after the 28 March 2005 earthquake, an earthquake of M_w 7.3 occurred in central Simeulue on 2 November 2002 [*DeShon et al.*, 2005]. At the four sites on Simeulue where we determined from imagery that there was

uplift (pink circles on Simeulue in Figure 5), the preearthquake images were all acquired prior to the November 2002 earthquake. (More details are provided in Table S1.) Hence the minimum uplift we report at those four sites is actually minimum net uplift that occurred during and between the 2002 and 2004 earthquakes. Uplift values determined from in situ microatoll measurements (Table S2), however, are clearly attributable to the 2004 earthquake. At a few sites in central Simeulue the coral microatolls record multiple uplift events. In those cases, the earlier uplift is on the order of ~20 cm or less, and we tentatively attribute it to the 2002 earthquake.

[16] We should note that only at a few localities were we able to provide both maximum and minimum constraints on the amount of uplift or subsidence; in most cases we were able to provide only minimum constraints on uplift or subsidence. This is because the remote sensing method is limited by the tidal range and, in particular, by the range of SSH among the satellite images that were acquired; in the Andaman and Nicobar islands this range is typically 1 m or less, and in Sumatra this range is typically less than 0.5 m. In any case where the amount of uplift or subsidence exceeded the SSH range, this method can only provide a minimum bound on the amount of tectonic elevation change. Information from other sources [e.g., *Bilham et al.*, 2005] suggests that elevation changes (uplift or subsidence) of several meters were widespread throughout the affected region. Hence any minimum bounds on uplift or subsidence stated in this paper should not be construed to represent or approximate the actual uplift or subsidence at that location; only the sign of the elevation change (up or down) at a location, and hence the constraints on the pivot line, should be considered robust. We must also caution against attempts to interpret any trends among the uplift (red) points or among the subsidence (blue) points in Figure 5. That a stated minimum uplift at one point might be greater than a stated minimum uplift at a second point does not imply that the uplift at the first point is greater than the uplift at the second point.

[17] In an attempt to provide some ground truth to the satellite imagery method and to our results we compared the results presented in Table S1 with recently released campaign GPS vertical vectors from 16 sites in the Andaman and Nicobar islands [*Jade et al.*, 2005; *Gahalaut et al.*, 2006] and a handful of sites in Sumatra [*Subarya et al.*, 2006]. For each of the GPS data located within roughly 50 km of at least one satellite imagery observation (i.e., for all of the GPS data from the Andaman and Nicobars but for only a few of the Sumatra data), we compared the GPS vertical vector to the closest imagery-based data. Our observations and inferences using satellite imagery and the tidal model were almost without exception consistent with the GPS data. At only two sites were the campaign GPS vertical vectors beyond the maximum or minimum bounds derived from our work.

[18] At one of the sites with discrepancy, HAVE on Havelock Island, Andaman Islands (12.03°N, 92.99°E), *Jade et al.* [2005] calculate an uplift of 0.6 ± 2.5 cm that they infer represents the coseismic displacement and postseismic movement through February 2005. They subtracted 15 months of inferred interseismic motion (which had a negligible vertical component) from the record, as the last preearthquake site occupation occurred in September 2003. The result, 0.6 ± 2.5 cm, is barely beyond the minimum subsidence of 3 to 4 cm allowed at the nearest sites, 4 to 9 km away, based on images acquired on 1 January 2004 and 4 February 2005 (Table S1). However, the reported value of *Jade et al.* [2005] may be suspect. *Gahalaut et al.* [2006] occupied station GG (Govindgarh; 12.036°N, 92.983°E), only ~1 km from HAVE, in March 2004 and January 2005, covering a shorter period of time and thereby allowing a more robust determination of the coseismic displacement vector. Their result, −18 ± 2 cm, is consistent with the imagery-based observations. The reason for the discrepancy between *Gahalaut et al.* [2006] and *Jade et al.* [2005] is unclear, but we note that our results for that vicinity are entirely consistent with the former and they are consistent with the latter within the stated (albeit conservative) ±14 cm (2σ) uncertainty resulting from the tide model.

[19] At the other site with discrepancy, Hut Bay (HB) on Little Andaman Island (10.696°N, 92.569°E), *Gahalaut et al.* [2006] report a coseismic elevation change of −26 ± 2 cm (i.e., 26 cm of subsidence), with successive site occupations in March 2004 and January 2005. In contrast, satellite images acquired on 1 January 2004 and 3 January 2005 (Table S1) indicate that the entire island of Little Andaman rose, with the eastern part (including Hut Bay) up at least 18 cm, although the nearest imagery-based datum to Hut Bay is more than 10 km away. Again, however, the GPS value may be suspect. Also using campaign GPS measurements, *Earnest et al.* [2005] determined that there was 36 cm of uplift at Hut Bay between August 2004 and early 2005, although the dates of their site occupations are not specified. Their result appears to be in conflict with that of *Gahalaut et al.* [2006] but is in complete agreement with our constraints. The reason for the discrepancy between *Gahalaut et al.* [2006] and *Earnest et al.* [2005] is unclear, but in further support of the imagery-based observations over the GPS observations of *Gahalaut et al.* [2006], *Bilham et al.* [2005] cite eyewitness reports of substantial (1−2 m, though this may be exaggerated) coseismic uplift at Hut Bay.

4. Conclusions

[20] We combine satellite imagery and ground observations of emerged and submerged coral reefs and microatolls and invoke a tidal model to resolve geodetic deformation associated with the 26 December 2004 Aceh-Andaman earthquake. We constrain the location of the pivot line separating regions of uplift and subsidence. Most of the rupture of the underlying megathrust must be west of this line. This line implies a rupture width that varies from slightly greater than 80 km to slightly greater than 120 km and a rupture length of ~1600 km, at least 100 km longer than that suggested by aftershock locations and by seismic inversions to date. Our method of using satellite imagery to recognize apparent color differences in coral reefs, of correlating these color differences with differences in elevation relative to SSH, and of using a tidal model to place quantitative bounds on coseismic uplift or subsidence is a novel approach that can be adapted to other forms of remote sensing and can be applied to other

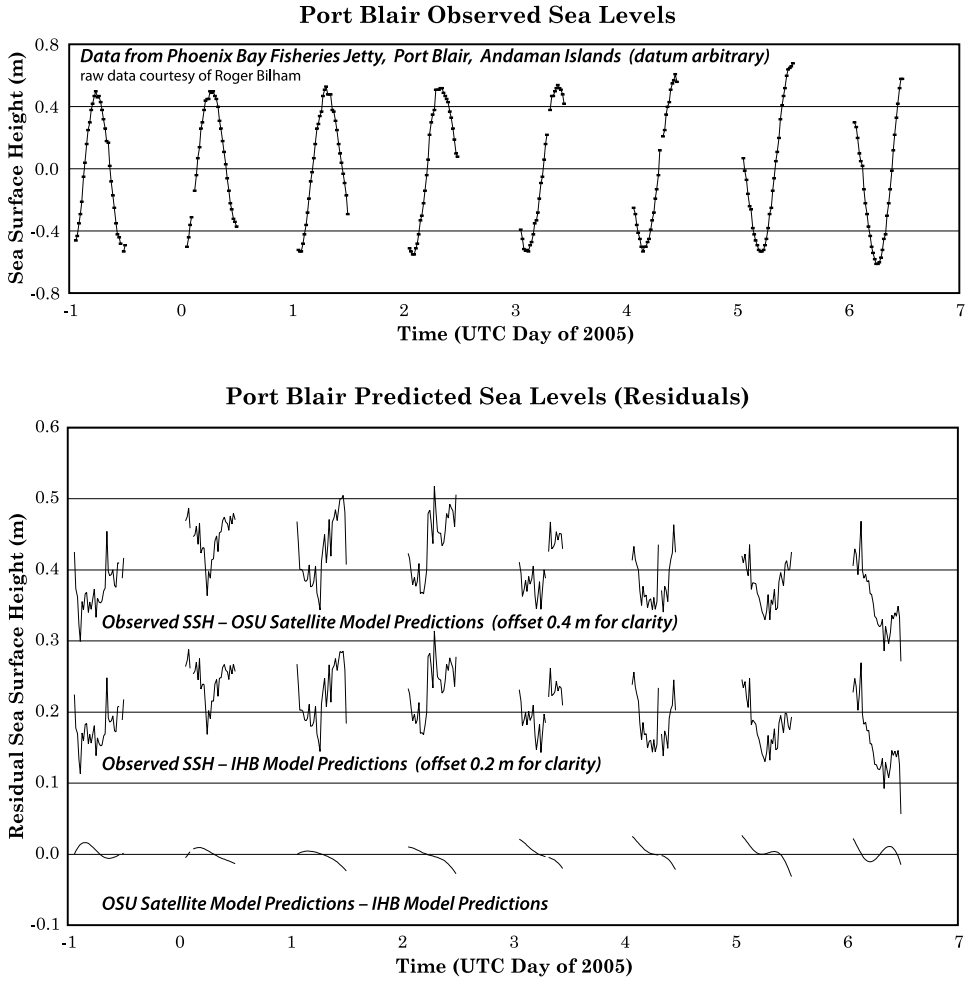

Figure A1. (top) Plot of the observed tides at Phoenix Bay Fisheries Jetty (PBFJ), Port Blair, Andaman Islands, for the period 31 December 2004 to 7 January 2005. (Day 0.0 corresponds to 1 January 2005, 0000:00 UTC.) (bottom) Residuals of the differences between the observations and the predictions of the Oregon State University (OSU) Bay of Bengal model, between the observations and the predictions of the International Hydrographic Bureau (IHB) model, and between the respective predictions of the OSU Bay of Bengal and IHB models. Each plot of residuals is offset vertically for clarity; also note the difference in the scale of the residual plots (Figure A1, bottom) in comparison to that of the observations (Figure A1, top). A significant portion of the residuals may be due to measurement errors or to imprecision in the tide gauge at PBFJ; still, the residuals fall within a 2σ uncertainty of ± 10 cm or less.

subduction zones in the tropics and perhaps elsewhere in the world.

Appendix A: Determination of Tide Heights

[21] In a comparison of preearthquake and postearthquake satellite imagery of reefs or coastal areas, in order to ascertain with certainty whether a particular area experienced uplift or subsidence, any variation in SSH due to tidal influences must be considered. In addition, as described in the body of this paper, if differences in the extent of reef exposure can be identified among the images of a location, then the difference in SSH between the images can be used to constrain the amount of uplift or subsidence.

[22] In order to determine the tidal height at each location of interest at the acquisition time of each satellite image we used the software package NLOADF [*Agnew*, 1997], along with harmonic tidal constituents extracted from the Oregon State University Regional Tidal Solutions (regional models based on satellite observations) for the Bay of Bengal and for Indonesia [*Egbert and Erofeeva*, 2002] (available at http://www.coas.oregonstate.edu/research/po/research/tide/region.html; hereinafter referred to as the Bay of Bengal and Indonesia models, respectively). The Bay of Bengal model covers the Andaman and Nicobar islands, and the Indonesia model covers Sumatra and its offshore islands, so these two models are sufficient for our study. The regional inverse solutions (including the Bay of Bengal and Indonesia models) have about the same residual magnitudes as the global solution TPXO.6 for the open ocean, but the regional solutions fit the data significantly better for areas with complex coastlines and bathymetry and are consequently preferred.

[23] To verify the harmonic tidal constituents extracted from the Bay of Bengal model, we compared the predictions of these constituents for Port Blair (in the Andaman Islands) for several arbitrary time periods with direct tide observations at the Phoenix Bay Fisheries Jetty (PBFJ) in Port Blair (Figure A1) and with the predictions from three ground-based sources: the Indian Tide Tables (ITT), the International Hydrographic Bureau (IHB), and the Admiralty Tide Tables (ATT). (See *Pugh* [2004, chapter 3] for a discussion of harmonic tidal constituents.) The ITT are published by the Survey of India and consist of predictions of times and heights of high and low tides at Port Blair, based on their (unknown to us) harmonic constituents, which are in turn based on tide gauge data; the predictions for January 1965 were read directly from the tables. The harmonic constituents of the IHB for Port Blair were derived from harmonic analysis of 41 years of tide gauge data (1880–1920) from the ITT; they are taken from *International Hydrographic Bureau* [1953, sheet 159]. The ATT are published by the British Admiralty and consist of harmonic constituents for Port Blair, also based on tide gauge data; the constituents for 1996 were chosen for this comparison. Note that the applicability of the ITT, the IHB, and the ATT predictions is limited to Port Blair and the few other locations for which tide gauge data exist; to assess the behavior of tides elsewhere in the Andaman and Nicobar islands and in Sumatra, a model based on satellite observations is more robust.

[24] Overall, the ITT and the IHB predictions should provide the closest approach to "ground truth" for the actual tidal heights, and the predictions for Port Blair of the ITT, the IHB, and the Bay of Bengal model are remarkably consistent with one another, lending credibility to the Bay of Bengal model. The standard deviation of the differences between the tidal observations at PBFJ and the predictions of the Bay of Bengal model is on the order of ±5 cm; likewise, for the year 2004 the standard deviation of the difference between the respective predictions of the Bay of Bengal model and the IHB constituents is roughly ±5 cm, and the maximum difference is under 20 cm. These values should provide a sense of the maximum likely errors in the Bay of Bengal model's predictions, at least for Port Blair. The ATT predictions differ somewhat from the others, so they will not be considered further. The Bay of Bengal model appears to be the best for use throughout the Andaman and Nicobar islands; the only location for which we did not use this model is for Port Blair itself, where the IHB tidal constituents should be most reliable. By extension of the foregoing discussion we considered the Indonesia regional model to be better than any ground-based local predictions for use throughout Sumatra.

[25] **Acknowledgments.** We thank Mohamed Chlieh, Chen Ji, Rich Briggs, and Rob McCaffrey for assistance and many insightful discussions. We are grateful to John Galetzka, Imam Suprihanto, and Bambang Suwargadi for data collection and invaluable field support in Indonesia and to Hidayat and Samsir of Derazona Air Services, our helicopter pilot and mechanic. We are very appreciative of Chris Goldfinger for collecting and sharing satellite imagery and of Roger Bilham for sharing data and making his manuscripts available to us, which benefited us tremendously. We thank JoAnne Giberson and Shaun Healy for ongoing GIS support. We also thank Vineet Gahalaut, Roger Bilham, and an anonymous reviewer for helpful reviews that led to substantial improvements in the paper. We acknowledge the use of QuickBird imagery made freely available by DigitalGlobe, and the use of IKONOS and SPOT 5 images acquired, processed, and made freely available by CRISP, National University of Singapore. This research was supported in part by the Gordon and Betty Moore Foundation and by NASA grant NAG5-10406. This is Caltech Tectonic Observatory contribution 23.

References

Agnew, D. C. (1997), NLOADF: A program for computing ocean-tide loading, *J. Geophys. Res.*, *102*, 5109–5110.

Ammon, C. J., et al. (2005), Rupture process of the 2004 Sumatra-Andaman earthquake, *Science*, *308*, 1133–1139.

Bilham, R., E .R. Engdahl, N. Feldl, and S. P. Satyabala (2005), Partial and complete rupture of the Indo-Andaman plate boundary 1847–2004, *Seismol. Res. Lett.*, *76*, 299–311.

Curray, J. R. (2005), Tectonics and history of the Andaman Sea region, *J. Asian Earth Sci.*, *25*, 187–228.

DeShon, H. R., E. R. Engdahl, C. H. Thurber, and M. Brudzinski (2005), Constraining the boundary between the Sunda and Andaman subduction systems: Evidence from the 2002 M_w 7.3 Northern Sumatra earthquake and aftershock relocations of the 2004 and 2005 great earthquakes, *Geophys. Res. Lett.*, *32*, L24307, doi:10.1029/2005GL024188.

Earnest, A., C .P. Rajendran, K. Rajendran, R. Anu, G. M. Arun, and P. M. Mohan (2005), Near-field observations on the co-seismic deformation associated with the 26 December 2004 Andaman-Sumatra earthquake, *Curr. Sci.*, *89*, 1237–1244.

Egbert, G. D., and S. Y. Erofeeva (2002), Efficient inverse modeling of barotropic ocean tides, *J. Atmos. Oceanic Technol.*, *19*, 183–204.

Gahalaut, V. K., B. Nagarajan, J. K. Catherine, and S. Kumar (2006), Constraints on 2004 Sumatra earthquake rupture from GPS measurements in Andaman-Nicobar islands, *Earth Planet. Sci. Lett.*, doi:10.1016/j.epsl.2005.11.051, in press.

International Hydrographic Bureau (1953), *Tides: Harmonic Constants*, *Int. Hydrogr. Bur. Spec. Publ., 26*, 121 pp., sheets 1–3055.

Jade, S., M. B. Ananda, P. D. Kumar, and S. Banerjee (2005), Co-seismic and post-seismic displacements in Andaman and Nicobar islands from GPS measurements, *Curr. Sci.*, *88*, 1980–1984.

Lay, T., et al. (2005), The great Sumatra-Andaman earthquake of 26 December 2004, *Science*, *308*, 1127–1133.

Miller, R. L., C. E. Del Castillo, and B. A. McKee (Eds.) (2005), *Remote Sensing of Coastal Aquatic Environments: Technologies, Techniques and Applications*, *Remote Sens. Digital Image Process.*, vol. 7, 347 pp., Springer, New York.

Natawidjaja, D. H., K. Sieh, S. N. Ward, H. Cheng, R. L. Edwards, J. Galetzka, and B. W. Suwargadi (2004), Paleogeodetic records of seismic and aseismic subduction from central Sumatran microatolls, Indonesia, *J. Geophys. Res.*, *109*, B04306, doi:10.1029/2003JB002398.

Plafker, G. (1972), Alaskan earthquake of 1964 and Chilean earthquake of 1960: Implications for arc tectonics, *J. Geophys. Res.*, *77*, 901–925.

Plafker, G., and J. C. Savage (1970), Mechanism of the Chilean earthquakes of May 21 and 22, 1960, *Geol. Soc. Am. Bull.*, *81*, 1001–1030.

Pugh, D. (2004), *Changing Sea Levels: Effects of Tides, Weather and Climate*, 280 pp., Cambridge Univ. Press, New York.

Subarya, C., M. Chlieh, L. Prawirodirdjo, J.-P. Avouac, R. McCaffrey, Y. Bock, K. Sieh, A. J. Meltzner, and D. H. Natawidjaja (2006), Static deformation of the great Aceh-Andaman earthquake, *Nature*, doi:10.1038/nature04522, in press.

Taylor, F. W., C. Frohlich, J. Lecolle, and M. Strecker (1987), Analysis of partially emerged corals and reef terraces in the central Vanuatu Arc: Comparison of contemporary coseismic and nonseismic with Quaternary vertical movements, *J. Geophys. Res.*, *92*, 4905–4933.

Vigny, C., et al. (2005), Insight into the 2004 Sumatra-Andaman earthquake from GPS measurements in southeast Asia, *Nature*, *436*, 201–206, doi:10.1038/nature03937.

Zachariasen, J., K. Sieh, F. W. Taylor, and W. S. Hantoro (2000), Modern vertical deformation above the Sumatran subduction zone: Paleogeodetic insights from coral microatolls, *Bull. Seismol. Soc. Am.*, *90*, 897–913.

M. Abrams, Jet Propulsion Laboratory 183-501, California Institute of Technology, 4800 Oak Grove Drive, Pasadena, CA 91109, USA.

D. C. Agnew, Scripps Institution of Oceanography 0225, University of California, San Diego, 9500 Gillman Drive, La Jolla, CA 92093, USA.

J.-P. Avouac, A. J. Meltzner, and K. Sieh, Tectonics Observatory, Division of Geological and Planetary Sciences, California Institute of Technology, Pasadena, CA 91125, USA. (meltzner@gps.caltech.edu; sieh@gps.caltech.edu)

K. W. Hudnut, U.S. Geological Survey, Pasadena Field Office, 525 South Wilson Avenue, Pasadena, CA 91106, USA.

D. H. Natawidjaja, Research Center for Geotechnology, Indonesian Institute of Sciences, Komplek LIPI Gd. 70, J1, Bandung 40135, Indonesia.

Auxiliary Material for Paper 2005JB003891

Uplift and subsidence associated with the great Aceh–Andaman earthquake of 2004

Aron J. Meltzner and **Kerry Sieh**
Tectonics Observatory, Division of Geological and Planetary Sciences,
California Institute of Technology,
Pasadena, California, USA

Michael Abrams
Jet Propulsion Laboratory,
California Institute of Technology,
Pasadena, California, USA

Duncan C. Agnew
Scripps Institution of Oceanography,
University of California, San Diego,
La Jolla, California, USA

Kenneth W. Hudnut
U.S. Geological Survey,
Pasadena, California, USA

Jean-Philippe Avouac
Tectonics Observatory, Division of Geological and Planetary Sciences,
California Institute of Technology,
Pasadena, California, USA

and **Danny H. Natawidjaja**
Research Center for Geotechnology,
Indonesian Institute of Sciences,
Bandung, Indonesia

Meltzner, A. J., K. Sieh, M. Abrams, D. C. Agnew, K. W. Hudnut, J.-P. Avouac, and D. H. Natawidjaja (2006), Uplift and subsidence associated with the great Aceh–Andaman earthquake of 2004, *J. Geophys. Res.*, 111, B02407, doi:10.1029/2005JB003891.

Introduction

This supplement consists of three tables that collectively constitute our data. Table S1 lists the constraints on vertical deformation that can be made from satellite imagery and the tidal model. Table S2 lists the estimates of vertical deformation on Simeulue that could be made from field observations in 2005, using uplifted coral microatolls in conjunction with the tidal model. Table S3 lists less quantitative information on coseismic subsidence on Simeulue, for two locations. Only some of the data listed in Tables S1–S3 are shown in map view on Fig. 5, whereas Tables S1–S3, collectively, are comprehensive.

1. **Table S1:** Vertical changes determined from satellite imagery.

1.1 Column "Latitude", degrees, latitude of the observation point, north of Equator.

1.2 Column "Longitude", degrees, longitude of the observation point, east of Greenwich.

1.3 Column "MinDeltaZ", minimum uplift (if positive) or maximum subsidence (if negative), in cm; "null" indicates that a given datum does not provide such constraint.

1.4 Column "MaxDeltaZ", maximum uplift (if positive) or minimum subsidence (if negative), in cm; "null" indicates that a given datum does not provide such constraint.

1.5 Column "2sigma", CONSERVATIVE (see text) 2-sigma uncertainty associated with both the minimum and maximum elevation changes, in cm. When stated as ± 14 cm, it is the uncertainty associated with the tidal model. When the uncertainty is listed as "0", the observation for that point is of submergence, i.e., of water connected to the ocean in a location where it would never have been previously; for these observations (all of which are in Aceh), the tidal model was not used.

Note added for Chapter 2 of AJM's thesis: Some values in this column have been changed. Values previously stated as ± 14 cm are now stated as ± 24 cm. These larger errors account for the fact that non-tidal sea level anomalies were not considered in the original imagery-based uplift and subsidence calculations. For more information, see Chapter 1 of this thesis.

1.6 Column "PreDate", acquisition date (yyyy/mm/dd, UTC) of the pre-earthquake image used for the final calculation of elevation change (additional pre-earthquake images may have been viewed for the study).

1.7 Column "PostDate", acquisition date (yyyy/mm/dd, UTC) of the post-earthquake image used for the final calculation of elevation change (additional post-earthquake images may have been viewed for the study).

1.8 Column "PreType", type of imagery of the pre-earthquake image used for the final calculation of elevation change (A: ASTER; I: IKONOS; Q: QuickBird; S: SPOT).

1.9 Column "PostType", type of imagery of the post-earthquake image used for the final calculation of elevation change (A: ASTER; I: IKONOS; Q: QuickBird; S: SPOT).

Points for which a minimum constraint on uplift or a minimum constraint on subsidence was determined are shown in map view on Fig. 5.

The following discussion might be useful for understanding Table S1:

a) If there is a positive number, say X, in column "MinDeltaZ", then any {uplift} greater than X is allowed.

b) If there is a negative number X in column "MinDeltaZ", then any {uplift} greater than X is allowed [this includes subsidence for which the absolute value of {elevation change} is less than abs(X), e.g., if X = –20 then 10 cm of subsidence is allowed; zero change or any positive uplift value would also be allowed].

c) If there is a number in column "MaxDeltaZ", call it Y, in addition to X in column "MinDeltaZ", then X < {elevation change} < Y.

d) If there is only a column "MaxDeltaZ" entry (only Y, no X) then {elevation change} < Y.

2. **Table S2:** Uplift on Simeulue determined from field measurements of coral microatolls.

2.1 Column "Latitude", degrees, latitude of the observation point, north of Equator.

2.2 Column "Longitude", degrees, longitude of the observation point, east of Greenwich.

2.3 Column "DeltaZ", uplift, in cm (none of these measurements were of subsidence).

2.4 Column "2sigma", estimated 2-sigma uncertainty associated with the calculation, in cm; sources of uncertainty include imprecision in the coral record, in the measurement technique, and in the tidal model.

2.5 Column "Date", date of measurement (yyyy/mm/dd).

These points are shown in map view on Fig. 5.

3. **Table S3:** Subsidence on Simeulue determined from field observations.

3.1 Column "Latitude", degrees, latitude of the observation point, north of Equator.

3.2 Column "Longitude", degrees, longitude of the observation point, east of Greenwich.

3.3 Column "DeltaZ", change in elevation, in cm.
(In Salur, we measured the depth of flooding of a well-drained locality where residents said water had never stood before, which effectively provides a minimum constraint on subsidence there; the uncertainty on this minimum constraint is difficult to assess.
In Busung, Gusong Bay, there is a rough estimate of subsidence from R. Peters, http://walrus.wr.usgs.gov/news/reportsleg1.html; no estimate of the uncertainty is available for this point, but it may be considerable.)

3.4 Column "Date", date of observation (yyyy/mm/dd).

3.5 Column "Location", name of location.

3.6 Column "Note", note on whether the value given in column "DeltaZ" is an estimate or a one-sided (minimum or maximum) constraint of the elevation change.

These points are shown in map view on Fig. 5.

Table S1: Vertical changes determined from satellite imagery

Latitude	Longitude	MinDeltaZ	MaxDeltaZ	2sigma*	PreDate	PostDate	PreType	PostType
14.862	93.682	20	null	*24*	2000/06/30	2005/01/10	A	I
14.015	93.236	23	null	*24*	2004/01/01	2005/01/03	A	A
13.967	93.237	23	null	*24*	2004/01/01	2005/01/03	A	A
13.648	93.081	38	null	*24*	2000/11/21	2005/01/03	A	A
13.611	93.060	38	null	*24*	2000/11/21	2005/01/03	A	A
13.619	93.033	38	null	*24*	2000/11/21	2005/01/03	A	A
13.674	93.029	38	null	*24*	2000/11/21	2005/01/03	A	A
13.647	92.984	38	null	*24*	2000/11/21	2005/01/03	A	A
13.599	92.909	39	null	*24*	2000/11/21	2005/01/03	A	A
13.568	92.895	39	null	*24*	2000/11/21	2005/01/03	A	A
13.575	93.038	35	null	*24*	2000/11/21	2005/01/03	A	A
13.571	92.996	35	null	*24*	2000/11/21	2005/01/03	A	A
13.541	92.964	35	null	*24*	2000/11/21	2005/01/03	A	A
13.516	92.922	35	null	*24*	2000/11/21	2005/01/03	A	A
13.537	92.882	38	null	*24*	2000/11/21	2005/01/03	A	A
13.493	92.879	38	null	*24*	2000/11/21	2005/01/03	A	A
13.473	92.898	38	null	*24*	2000/11/21	2005/01/03	A	A
13.389	92.846	38	null	*24*	2000/11/21	2005/01/03	A	A
13.354	92.841	37	null	*24*	2000/11/21	2005/01/03	A	A
13.199	92.825	36	null	*24*	2000/11/21	2005/01/03	A	A
13.167	92.800	36	null	*24*	2000/11/21	2005/01/03	A	A
13.108	92.819	36	null	*24*	2000/11/21	2005/01/03	A	A
13.092	92.808	37	null	*24*	2000/11/21	2005/01/03	A	A
13.025	92.799	37	null	*24*	2000/11/21	2005/01/03	A	A
13.478	93.045	21	null	*24*	2000/11/21	2005/01/03	A	A
13.419	93.074	21	null	*24*	2000/11/21	2005/01/03	A	A
13.431	93.113	17	null	*24*	2004/01/01	2005/01/03	A	A
13.400	93.099	17	null	*24*	2004/01/01	2005/01/03	A	A
13.296	93.090	17	null	*24*	2004/01/01	2005/01/03	A	A
13.222	93.061	17	null	*24*	2004/01/01	2005/01/03	A	A
13.117	93.041	17	null	*24*	2004/01/01	2005/01/03	A	A
13.027	92.978	1	null	*24*	2000/11/21	2005/02/04	A	A
12.894	92.919	1	null	*24*	2000/11/21	2005/02/04	A	A
12.894	92.919	null	17	*24*	2004/01/01	2005/01/03	A	A
13.111	92.709	10	null	*24*	2000/11/21	2005/02/04	A	A
13.062	92.707	10	null	*24*	2000/11/21	2005/02/04	A	A
12.936	92.770	40	null	*24*	2000/11/21	2005/01/03	A	A
12.864	92.734	40	null	*24*	2000/11/21	2005/01/03	A	A
12.752	92.718	40	null	*24*	2000/11/21	2005/01/03	A	A
12.717	92.726	39	null	*24*	2000/11/21	2005/01/03	A	A
12.641	92.710	39	null	*24*	2000/11/21	2005/01/03	A	A
12.583	92.688	39	null	*24*	2000/11/21	2005/01/03	A	A
12.569	92.710	39	null	*24*	2000/11/21	2005/01/03	A	A
12.557	92.690	39	null	*24*	2000/11/21	2005/01/03	A	A
12.504	92.684	39	null	*24*	2000/11/21	2005/01/03	A	A
12.467	92.705	38	null	*24*	2000/11/21	2005/01/03	A	A

Table S1: Vertical changes determined from satellite imagery

Latitude	Longitude	MinDeltaZ	MaxDeltaZ	2sigma*	PreDate	PostDate	PreType	PostType
12.413	92.705	38	null	*24*	2000/11/21	2005/01/03	A	A
12.378	92.706	37	null	*24*	2000/11/21	2005/01/03	A	A
12.331	92.705	37	null	*24*	2000/11/21	2005/01/03	A	A
12.852	92.950	1	null	*24*	2000/11/21	2005/02/04	A	A
12.852	92.950	null	17	*24*	2004/01/01	2005/01/03	A	A
12.405	92.964	null	-4	*24*	2004/01/01	2005/02/04	A	A
12.371	92.950	null	-4	*24*	2004/01/01	2005/02/04	A	A
12.257	92.704	8	null	*24*	2000/11/21	2005/02/04	A	A
12.257	92.704	null	36	*24*	2000/11/21	2005/01/03	A	A
12.221	92.671	9	null	*24*	2000/11/21	2005/02/04	A	A
12.221	92.671	null	37	*24*	2000/11/21	2005/01/03	A	A
12.133	92.639	9	null	*24*	2000/11/21	2005/02/04	A	A
12.035	92.625	9	null	*24*	2000/11/21	2005/02/04	A	A
11.930	92.551	10	null	*24*	2000/11/21	2005/02/04	A	A
11.877	92.529	10	null	*24*	2000/11/21	2005/02/04	A	A
11.804	92.525	10	null	*24*	2000/11/21	2005/02/04	A	A
11.662	92.603	null	-30	*24*	2004/12/02	2005/01/03	A	A
11.497	92.570	null	-30	*24*	2004/12/02	2005/01/03	A	A
12.153	92.830	null	-46	*24*	2004/12/02	2005/01/03	A	A
12.071	92.789	null	-45	*24*	2002/01/11	2005/02/04	A	A
11.702	92.754	null	-63	*24*	2004/12/02	2005/02/04	A	A
11.669	92.710	null	-66	*24*	2004/12/02	2005/02/04	A	A
11.649	92.670	null	-66	*24*	2004/12/02	2005/02/04	A	A
11.548	92.746	null	-3	*24*	2004/01/01	2005/02/04	A	A
12.105	92.954	null	-3	*24*	2004/01/01	2005/02/04	A	A
12.009	93.016	null	-4	*24*	2004/01/01	2005/02/04	A	A
11.992	92.929	null	-4	*24*	2004/01/01	2005/02/04	A	A
11.957	92.971	null	-4	*24*	2004/01/01	2005/02/04	A	A
11.924	93.003	null	-4	*24*	2004/01/01	2005/02/04	A	A
11.498	92.619	null	-23	*24*	2002/01/11	2005/02/04	A	A
11.463	92.614	null	-23	*24*	2002/01/11	2005/02/04	A	A
11.388	92.564	null	21	*24*	2004/01/01	2005/01/03	A	A
11.305	92.720	null	16	*24*	2004/01/01	2005/01/03	A	A
10.982	92.670	null	18	*24*	2004/01/01	2005/01/03	A	A
11.596	92.219	30	null	*24*	2000/11/21	2005/02/20	A	A
11.585	92.280	30	null	*24*	2000/11/21	2005/02/20	A	A
11.528	92.216	30	null	*24*	2000/11/21	2005/02/20	A	A
11.520	92.288	30	null	*24*	2000/11/21	2005/02/20	A	A
10.972	92.236	29	null	*24*	2000/11/21	2005/02/20	A	A
10.899	92.535	21	null	*24*	2004/01/01	2005/01/03	A	A
10.801	92.592	21	null	*24*	2004/01/01	2005/01/03	A	A
10.830	92.431	21	null	*24*	2004/01/01	2005/01/03	A	A
10.781	92.378	7	null	*24*	2002/01/11	2005/01/03	A	A
10.662	92.384	22	null	*24*	2004/01/01	2005/01/03	A	A
10.609	92.410	22	null	*24*	2004/01/01	2005/01/03	A	A

Table S1: Vertical changes determined from satellite imagery

Latitude	Longitude	MinDeltaZ	MaxDeltaZ	2sigma*	PreDate	PostDate	PreType	PostType
10.546	92.382	22	null	*24*	2004/01/01	2005/01/03	A	A
10.523	92.391	18	null	*24*	2004/01/01	2005/01/03	A	A
10.511	92.481	18	null	*24*	2004/01/01	2005/01/03	A	A
10.511	92.543	18	null	*24*	2004/01/01	2005/01/03	A	A
10.783	92.608	18	null	*24*	2004/01/01	2005/01/03	A	A
9.211	92.720	null	-9	*24*	2003/11/30	2005/08/15	A	A
9.118	92.798	null	-7	*24*	2003/11/30	2005/08/15	A	A
9.166	92.830	null	-7	*24*	2003/11/30	2005/08/15	A	A
8.460	93.068	null	3	*24*	2002/01/04	2005/03/24	A	A
8.311	93.137	null	-0.4	*24*	2002/01/04	2005/03/24	A	A
8.232	93.117	null	-8	*24*	2002/01/04	2005/03/24	A	A
8.232	93.232	null	22	*24*	2002/01/04	2005/02/13	A	A
8.002	93.328	null	3	*24*	2002/01/04	2004/12/28	A	S
7.890	93.339	null	-32	*24*	2001/07/21	2004/12/28	A	S
8.214	93.500	null	-39	*24*	2001/07/21	2004/12/28	A	S
8.080	93.601	null	-43	*24*	2001/07/21	2004/12/28	A	S
7.470	93.623	null	-22	*24*	2001/07/21	2005/01/28	A	A
7.401	93.701	null	-21	*24*	2001/07/21	2005/01/28	A	A
7.373	93.686	null	-21	*24*	2001/07/21	2005/01/28	A	A
7.371	93.648	null	-21	*24*	2001/07/21	2005/01/28	A	A
7.204	93.757	null	-46	*24*	2000/10/29	2005/02/06	A	A
7.180	93.680	null	-46	*24*	2000/10/29	2005/02/06	A	A
7.136	93.673	null	-38	*24*	2000/10/29	2005/02/06	A	A
7.104	93.663	null	-42	*24*	2000/10/29	2005/01/05	A	A
7.074	93.667	null	-42	*24*	2000/10/29	2005/01/05	A	A
7.026	93.674	null	-44	*24*	2000/10/29	2005/01/05	A	A
6.985	93.735	null	-44	*24*	2000/10/29	2005/01/05	A	A
6.920	93.774	null	-44	*24*	2000/10/29	2005/01/05	A	A
6.821	93.823	null	-67	*24*	2000/10/29	2005/01/05	A	A
6.820	93.877	null	-67	*24*	2000/10/29	2005/01/05	A	A
7.173	93.885	null	-10	*24*	2000/10/29	2005/01/28	A	A
3.014	95.406	28	null	*24*	2001/11/19	2005/03/03	A	A
2.548	95.937	13	null	*24*	2002/10/30	2005/01/30	A	A
2.569	95.992	8	null	*24*	2001/11/28	2004/12/29	A	A
2.519	96.133	5	null	*24*	2001/11/28	2005/02/24	A	A
2.470	96.206	4	null	*24*	2001/11/28	2005/01/23	A	A
2.415	96.225	-17	null	*24*	2003/10/17	2005/01/23	A	A
2.333	96.445	-28	null	*24*	2003/03/07	2005/02/24	A	A
2.405	96.487	-29	null	*24*	2003/03/07	2005/01/23	A	A
2.405	96.487	null	6	*24*	2003/01/18	2005/01/23	A	A
2.025	97.117	-13	null	*24*	2000/08/30	2005/02/08	A	A
2.108	97.087	-14	null	*24*	2000/08/30	2005/02/08	A	A
2.227	97.117	-14	null	*24*	2000/08/30	2005/02/08	A	A
2.253	97.198	-14	null	*24*	2000/08/30	2005/02/08	A	A
2.320	97.213	-15	null	*24*	2000/08/30	2005/02/08	A	A

Table S1: Vertical changes determined from satellite imagery

Latitude	Longitude	MinDeltaZ	MaxDeltaZ	2sigma*	PreDate	PostDate	PreType	PostType
5.646	95.414	null	0	0	null	2004/12/30	null	Q
5.626	95.400	null	0	0	null	2004/12/30	null	Q
5.592	95.360	null	0	0	null	2004/12/30	null	Q
5.577	95.333	null	0	0	null	2004/12/30	null	Q
5.560	95.300	null	0	0	null	2004/12/30	null	Q
5.548	95.270	null	0	0	null	2004/12/30	null	Q
5.542	95.252	null	0	0	null	2004/12/30	null	Q
5.552	95.235	null	0	0	null	2004/12/30	null	Q
5.508	95.277	null	0	0	null	2004/12/30	null	Q
5.498	95.249	null	0	0	null	2004/12/30	null	Q
4.600	95.622	null	0	0	2002/01/06	2005/03/19	A	A
3.547	97.000	-9	null	*24*	2003/03/07	2005/03/12	A	A
3.455	97.052	-9	null	*24*	2003/03/07	2005/03/12	A	A
3.338	97.125	-22	null	*24*	2002/01/31	2005/02/08	A	A
3.257	97.192	-22	null	*24*	2002/01/31	2005/02/08	A	A
2.907	97.441	null	10	*24*	2002/01/31	2005/03/05	A	A
2.871	97.515	null	1	*24*	2002/02/16	2005/03/05	A	A
2.254	97.935	null	42	*24*	2000/07/13	2005/02/01	A	A
2.188	98.038	null	42	*24*	2000/07/13	2005/02/01	A	A
2.146	98.125	null	42	*24*	2000/07/13	2005/02/01	A	A
2.096	98.176	null	42	*24*	2000/07/13	2005/02/01	A	A
2.027	98.266	null	43	*24*	2000/07/13	2005/02/01	A	A
2.010	98.373	null	44	*24*	2000/07/13	2005/02/01	A	A
1.972	98.348	null	43	*24*	2000/07/13	2005/02/01	A	A

* *Values in the '2sigma' column in italics (i.e., those entries listed as '24') have been modified from the original table published by Meltzner et al. [2006].*

These larger errors account for the fact that non-tidal sea level anomalies were not considered in the imagery-based uplift and subsidence calculations of Meltzner et al. [2006].

For more information, see Chapter 1 of this thesis.

Table S2: Uplift on Simeulue from field measurements of coral microatolls

Latitude	Longitude	DeltaZ*	2sigma*	Date
2.84368	95.91775	*22*	*23*	2005/01/18
2.91409	95.83584	*34*	*18*	2005/01/17
2.92359	95.80408	*46*	*23*	2005/02/05
2.86137	95.76308	*132*	*23*	2005/01/18
2.80665	95.71368	*148*	*18*	2005/01/17
2.74940	95.71628	*147*	*18*	2005/01/17
2.70852	95.76263	*131*	*18*	2005/01/17
2.61317	95.87225	*101*	*23*	2005/01/18
2.56913	95.99237	*48*	*23*	2005/01/18
2.54773	95.93723	*46*	*23*	2005/01/18

* *Values in the 'DeltaZ' and '2sigma' columns in this table are no longer considered the best estimates of uplift at these locations; they have since been modified slightly, and the errors have been reduced.*

Revised estimates of 2004 uplift on northern Simeulue are provided in Chapters 3 and 4 of this thesis; a detailed discussion of the revisions is provided in Chapter 4.

Table S3: Subsidence on Simeulue determined from field observations

Latitude	Longitude	DeltaZ	Date	Location	Note
2.443	96.241	-30	2005/01/18	Salur	minimum subsidence
2.392	96.332	-50	2005/04/08	Gusong	estimated subsidence